2023 IEEE International Conference on Robotics and Automation (ICRA 2023)
May 29 - June 2, 2023. London, UK

In-Hand Manipulation in Power Grasp: Design of an Adaptive Robot Hand with Active Surfaces

Yilin Cai, Shenli Yuan

Abstract— **This paper describes the development of BACH (Belt–Augmented Compliant Hand), a compliant robotic hand equipped with active surfaces. The hand can securely grasp an object using power grasp and simultaneously manipulate the grasped object. The hand consists of three identical fingers, each with an actuated timing belt wrapped around a Fin Ray based compliant finger backbone. Each finger is mounted on a compliant pivot joint allowing for further adaptability. The combination of compliant mechanisms and active surfaces allows the hand to perform dexterous in-hand manipulation with great robustness. Multiple analyses were conducted to optimize and validate the design of BACH. The hand was experimentally tested for grasping and manipulating objects of various geometries and sizes, and it demonstrated highly robust and efficient in-hand manipulation capabilities.**

I. Introduction

Robot in-hand manipulation refers to robots' ability to move a grasped object with respect to the robot hand. [1] In most common in-hand manipulation scenarios, the object being manipulated needs to be grasped in the hand during hand movement, which leads to a trade-off between grasp stability and manipulation dexterity. On one hand, the goal of in-hand manipulation is to reposition or reorient the grasped object, which, by definition, requires relative motions between the object and the hand. As a result, precision grasp is significantly more common compared to power grasp for in-hand manipulation applications regardless of the types of contact (fixed or rolling) between the robot fingers and the object. On the other hand, while precision grasp offers better dexterity for manipulation because of fewer constraints imposed on a grasped object, it does not provide a similar level of grasp stability compared to a power grasp. Therefore, loss of grasp would often occur during in-hand manipulation.

Different attempts to improve manipulation robustness directly or indirectly tackled this issue. The first method employed support surfaces [2], [3], where an object is placed on support surfaces during manipulation rather than being securely grasped by the fingers. Another method used active surfaces [4], [5], which despite using precision grasp, eliminates the need for finger-gaiting and therefore avoids transient states when the finger breaks and establishes contact with the object during manipulation. While these approaches have demonstrated some success, most of them do not provide sufficient grasp stability for robust in-hand manipulation.

This work was supported by SRI International. *(Corresponding author: Shenli Yuan.)*

Yilin Cai is with the Robotics Institute, Carnegie Mellon University, Pittsburgh, PA 15213 USA (email: yilincai@andrew.cmu.edu), Shenli Yuan is with SRI International, Menlo Park, CA 94025 USA (email: shenli.yuan@sri.com).

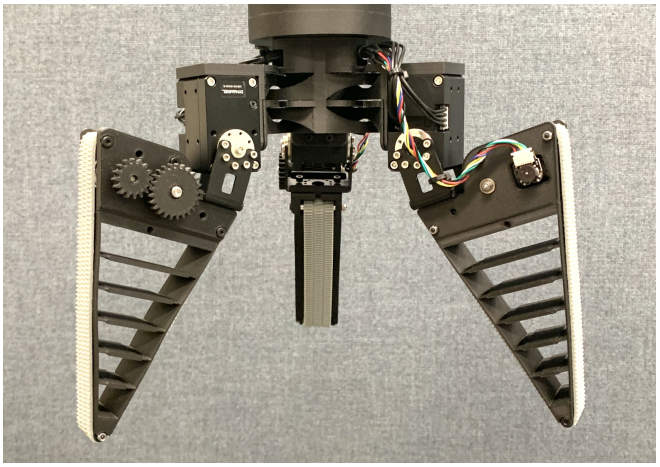

Fig. 1. The BACH prototype consisting of three compliant fingers with active surfaces.

Contrary to the articulated robot hands that provide high dexterity, underactuated hands can conform to a wide range of objects through their mechanical compliance [6]–[8]. While they provide a superior grasp stability without the need for a complex control scheme, their inherent lack of controllability makes it challenging for them to perform in-hand manipulation.

In this work, we developed BACH (Belt–Augmented Compliant Hand) (Fig. 1) - a new type of robot hand that uses compliant mechanisms that allow the hand to passively conform to different object shapes, and simultaneously uses active surfaces to achieve robust and dexterous in-hand manipulation. The paper presents previous research related to this work in Section II. Section III describes the design of the BACH. Section IV lays out analysis results related to grasping and in-hand manipulation. Section V shows various real-world experiments and discusses the results. Section VI provides conclusions and possible future directions.

II. Related Work

A. Robot Graspers with Active Surfaces

Usage of conveyor surfaces, or active surfaces, can enhance the manipulation capability of a robotic grasper [9]. Robot hands with active surfaces (e.g., [4], [5], [10]–[12]) can impart motion to grasped objects without needing to break contacts, contrary to the conventional finger-gaiting technique. While traditional linkage-based hands can also achieve manipulation through rolling contact, the range of

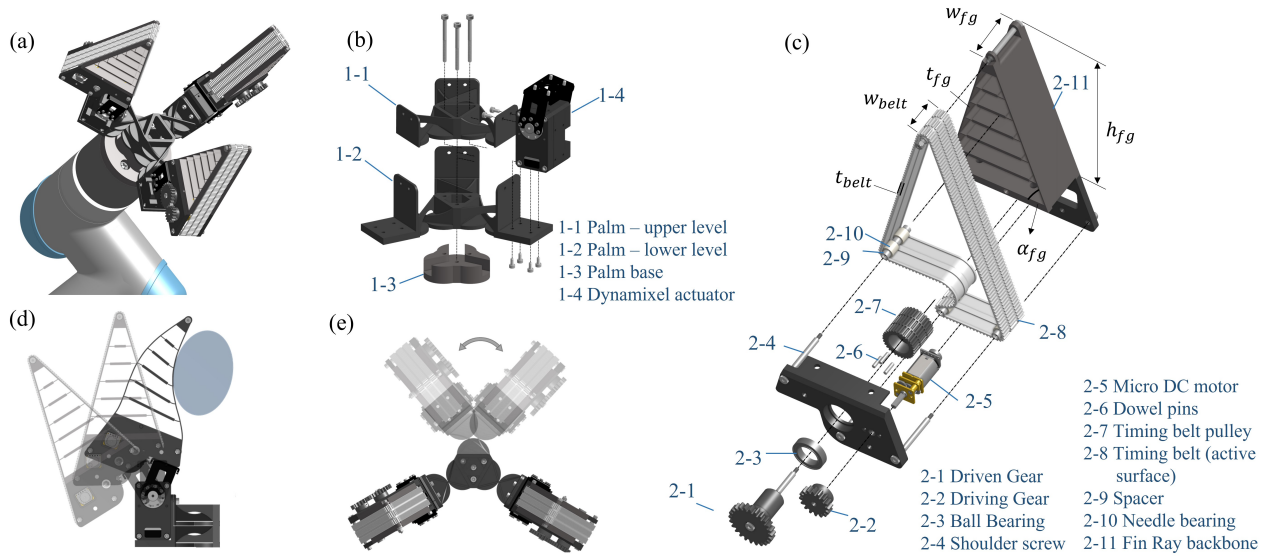

Fig. 2. A CAD model of the BACH: (a) An illustration of the BACH mounted on a UR5 robot. (b) An exploded view of the palm. (c) An exploded view of the finger with active surface. (d) Compliant grasping of the finger. (e) Adaptive pivot joints

motion is limited due to the kinematic constraints, restricting its use in these types of applications. Most robot hands with active surfaces are fully actuated and use precision grasp to maximize dexterity at the cost of lower power grasp stability. A more recent work [12] uses underactuated fingers with an active surface in the attempt to provide sufficient grasp stability and limited dexterity for in-hand manipulation.

B. Underactuated Hand

Underactuated hands such as [7], [13]–[16], focus on achieving grasping and manipulation capabilities with fewer actuated DoF compared to mechanical DoF. Underactuated fingers can passively conform to various shapes of objects, which allows them to securely grasp different objects without complex control schemes. In general, underactuation sacrifices controllability for its mechanical intelligence [17], making it more challenging to achieve in-hand manipulation.

C. Compliant Hand and Compliant Mechanisms

Compliant or soft hands (e.g., [18]–[20]), a category of robot hands built using compliant materials, have infinite DoF and can be considered a more extreme design compared to traditional linkage-based underactuated hands. The inherent compliance of the material makes them suitable for safe and delicate operations, but it makes it more difficult for them to perform highly dexterous manipulation.

Many compliant hands use compliant mechanisms (CM) that allow relative motions between rigid links by deforming compliant elements (hinges) connecting the links [21]. CM have become increasingly popular due to their high precision, monolithic structure, low friction, and simplified fabrication process [22], [23].

By using a flexural hinge as the finger joint, various compliant robot hands have been designed [24]–[26] that provide both firm power grasps and low-stiffness fingertip grasps. The entire finger can be designed as a compliant backbone and can bend into different shapes [27]. In addition to fingers, a bio-inspired compliant robot wrist was proposed in [28], whose mobility was achieved by employing two pairs of tendon-actuated, contact-aided, cross-axial flexural pivots (CAFP) [28]. CM not only serves as a replacement for a traditional revolute joint; it also generates translational motions, varies centers of rotation, and forms complex multi-bar mechanisms.

III. Design

The BACH features two key components: a compliant palm and three identical compliant fingers with active surfaces. Each finger has two actuated DoF. The base DoF is a revolute joint directly driven by a Robotis Dynamixel XM430-W350 actuator. This DoF moves the whole finger assembly, contributing to the grasping motion. The other DoF (surface DoF) is a Micro DC Motor driving a custom-designed belt to augment the compliant finger backbone with active surface. The three fingers are arranged in a centrosymmetric manner on a compliant palm. The physical parameters for the BACH are listed in Table. I

A. Finger Design

The first question we considered when designing the BACH involved the directions of motions that we want it to impart on a grasped object. Robot graspers are commonly mounted on different types of robot arms that often feature a rotating wrist, allowing the grasped object to be rotated around the wrist axis directly. Therefore, we decided to focus the design on reorienting an object around the axes orthogonal to the wrist axis. This motivated two important design decisions: (1) we needed at least three fingers to allow the object to be manipulated around multiple axes orthogonal to the wrist, and (2) if we considered a typical finger-wrist setup in which the joints of the fingers are orthogonal to the wrist, the direction of motion provided by the active surface should be along the length of the fingers.

TABLE I

SPECIFICATIONS OF THE BACH

Symbol	Description	Value
w_{fg}	Fin Ray finger width [mm]	30
h_{fg}	Fin Ray finger height [mm]	100
α_{fg}	Fin Ray finger side angle [$\circ$]	74.4
n_{fg}	Number of ray in a Fin Ray finger	5
t_{tg}	Thickness of the Fin Ray side [mm]	0.8
w_{belt}	Width of the timing belt [mm]	19
t_{belt}	Thickness of the timing belt [mm]	0.5
$w_{1t,2t}$	Dimensions of the fixed end of CAFP [mm]	0.50
$w_{1b,2b}$	Dimensions of the moving end of CAFP [mm]	0.50
$\beta_{1,2}$	Tilting angles of the flexural beams 1,2 [$^\circ$]	46
t_b	Maximum thickness of the flexural beam [mm]	13
t_m	Minimum thickness of the flexural beam [mm]	5.5
b	In-plane width of the flexural beam [mm]	0.8

We decided to use compliant mechanisms to provide a higher degree of underactuation and lower friction, and potentially reduce the design complexity compared to a linkage-based mechanism. However, the lack of discrete flanges requires the active surface to be wrapped around the entire surface of the finger, and the concavity created by finger curling would result in the belt detaching from the finger surface, negating the benefit of underactuation. This is why we selected the passive Fin Ray mechanism [29], [30] to achieve finger compliance. Unlike many other actively curling mechanisms (whether pneumatic or cable driven), the Fin Ray mechanism would not bend without the presence of an external force. This means that, despite the concavity it creates during curling, the grasped object will force the belt on to the finger, filling the concavity and preventing the belt from detaching, because the belt is sandwiched between the finger and the object (Fig. 2(d)).

As shown in Fig. 2(c), the Fin Ray mechanism is augmented with a custom designed timing belt 3D-printed with Thermoplastic polyurethane (TPU, Polymaker PolyFlex TPU90) and 100% infill. The grooves on the timing belt are relatively shallow because it is simultaneously used as a contact surface to provide a high friction for object manipulation. The belt is routed around the timing belt pulley to maximize the contact area between the pulley and the belt. The other side of the belt is designed to match the shape of the idlers. Each idler is made with two needle bearings that would latch the belt in the lateral direction but allow free longitudinal motion of the belt.

B. Palm Design

The palm consists of three joints, each formed by two levels of cross-axis flexural pivots (CAFPs). For each joint, the two levels of CAFPs have an opposite cross-bar arrangement and a pair of contact-aided members that compensate for each other's twisting tendencies, ensuring that only the finger pivoting motion is allowed. These two layers are designed as separate components to facilitate 3D printing. This palm design allows each finger to pivot up to 90°. Further analysis of this mechanism is presented in Section IV.

Aside from the custom belt 3D-printed with TPU, the rest of the custom components are 3D-printed using Onyx™ (micro carbon-filled nylon) on a Markforged Onyx One™ 3D printer with 37% infill. All the compliant features, such as the Fin Ray wall and the cross-bars, have relatively thin geometries, making them effectively 100% infilled. Therefore, these dimensions can only be multiples of the horizontal resolution of the printer.

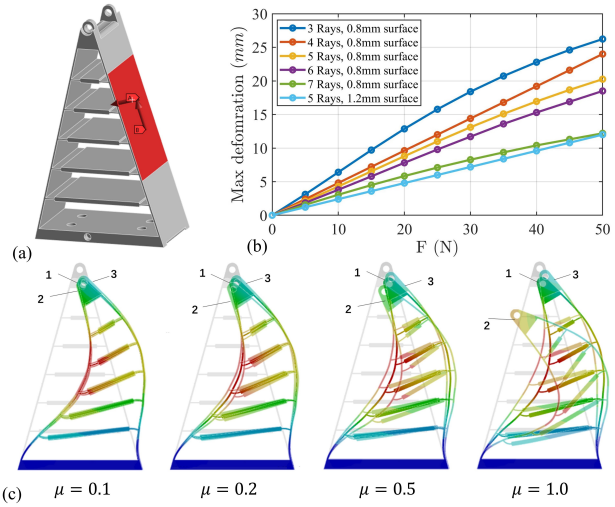

Fig. 3. FEM simulation of the Fin Ray finger. (a) Simulation setup where normal force and friction force are applied to the finger surface. (b) Maximum deformation of fingers with different Fin Ray parameters. (c) Comparison of finger deformations with and without friction. (1. No friction 2. Friction pointing downward 3. Friction pointing upward.)

IV. ANALYSIS

A. Finger Compliance

Prior works have developed analytical models to describe the properties of the fin ray effect [31], [32]. However, to achieve more accurate and comprehensive analysis, in this work we studied the properties of the compliant finger design through Finite Element Method (FEM) simulation using *ANSYS Workbench* Static Structural module. Based on the material properties used for finger production, we modeled the simulation using nylon with a Young's modulus of 1.7 GPa and a Poisson's ratio of 0.3.

1) Fin Ray design: Two of the major design parameters that affect the compliance of the Fin Ray backbone are the number of rays and the thickness of the sides. Fig. 3(b) shows the effect of these parameters on the maximum finger deformation when a 50 N force is applied uniformly on a pre-defined contact area. As we expected, the finger becomes more compliant as we reduce the number of rays and the thickness of the sides. We selected the 5-ray and $0.8mm$-thick sides in our final design for an optimal balance between compliance and strength.

2) Finger-belt interaction: In addition to the compliance analysis on the Fin Ray backbone, we also investigated how the motion of the active surface would affect finger compliance. As the active surface is in direct contact with the finger backbone, it inevitably introduces friction when moving with respect to the surface of the Fin Ray backbone. As shown in Fig. 3(c), the friction from the active surface has minimal influence on finger compliance regardless of its directions of motions, unless with an extreme coefficient of

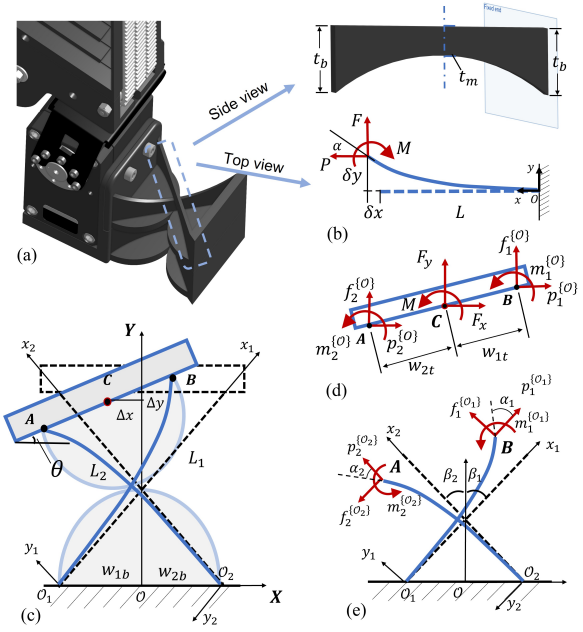

Fig. 4. Kinetostatics modeling of single CAFP joint. (a) CAFP joint on the BACH. (b) Deflection of a simple beam subject to external load F, P and M applied at its free end. (c) The deflection of CAFP under external load. (d,e) Free-body-diagrams of the CAFP under external load.

friction. As the inner surface of the belt is smooth enough, based on the analysis, we can expect the friction will bring a deviation less than 10%.

Another belt-finger interaction is potential finger buckling due to the sharp angle of the fingertip and the belt tension. Our buckling analysis in *ANSYS* shows that the critical force causing first-order modal buckling is 53.2 N. As the angle of the finger is 31.3°, it will take 27.5 N of belt tension to result in buckling, which would have already resulted in significant elongation of the TPU belt.

B. Pivot Joints

As introduced in Section III, the palm consists of three passive pivot joints each formed by two levels of CAFPs. The fixed and moving end of the joint are connected with two crossing beams, which provide an additional DoF of compliance for the finger. In this subsection, we will model and analyze the pivot joint for design optimization.

1) Single CAFP modeling: We use the Beam-Constraint Model (BCM), a closed-form method capable of capturing nonlinearities of a flexible beams in their intermediate deflection range (i.e., $10\% - 15\%$ of the length), to model kinetostatics of the single CAFP [33], [34]. The axial and transversal deflections Δx_i, Δy_i and end slope α_i of each beam, subject to an external transverse force F_i, an axial force P_i, and a moment M_i applied at its moving end, is modeled by the following parametric equations:

$$[f_i\ m_i]^T = \mathbf{G_c}\delta\boldsymbol{l_i} + p_i\mathbf{P_c}\delta\boldsymbol{l_i} + p_i^2\mathbf{Q_c}\delta\boldsymbol{l_i} \quad (1)$$

$$\delta x_i = \frac{t_i^2 p_i}{12L_i^2} - \frac{1}{2}\delta\boldsymbol{l_i}^T\mathbf{U_c}\delta\boldsymbol{l_i} - p_i\delta\boldsymbol{l_i}^T\mathbf{V_c}\delta\boldsymbol{l_i} \quad (2)$$

where $i = 1, 2$ is the index of the flexural beam, $\delta\boldsymbol{l_i} = [\delta y_i\ \alpha_i]^T$, f_i, p_i, m_i are the load parameters, $\delta x_i, \delta y_i$ are the deflection parameters normalized with respect to the beam length L_i, and I_i is the area moment of inertia:

$$m_i = \frac{M_i L_i}{EI_i}, f_i = \frac{F_i L_i^2}{EI_i}, p_i = \frac{P_i L_i^2}{EI_i}, \delta x_i = \frac{\Delta x_i}{L_i}, \delta y_i = \frac{\Delta y_i}{L_i} \quad (3)$$

and $\mathbf{G_c}$, $\mathbf{P_c}$, $\mathbf{U_c}$, $\mathbf{Q_c}$ and $\mathbf{V_c} \in \mathbb{R}^{2\times 2}$ are constant coefficients [34].

The fixed and the moving ends of the cross-beam joint are assumed to be rigid bodies and Fig. 4 demonstrates the deformed joint under the external load F, P, M applied to the center of the moving link (point **C**). As shown in Fig. 4(d), the force and moment equilibrium of each joint can be written as:

$$\begin{aligned} &M + (w_{1t} + w_{2t})\frac{EI_2}{L_2^2}\left[\mathrm{s}\theta\ -\mathrm{c}\theta\right]\left[p_2^{\{\mathcal{O}\}}\ f_2^{\{\mathcal{O}\}}\right]^T \\ &+w_{1t}\left[\mathrm{s}\theta\ -\mathrm{c}\theta\right][F_x\ F_y]^T - \frac{EI_1}{L_1}m_1 - \frac{EI_2}{L_2}m_2 = 0 \end{aligned} \quad (4)$$

$$[F_x\ F_y]^T + \frac{EI_1}{L_1^2}\left[p_1^{\{\mathcal{O}\}}\ f_1^{\{\mathcal{O}\}}\right]^T + \frac{EI_2}{L_2^2}\left[p_2^{\{\mathcal{O}\}}\ f_2^{\{\mathcal{O}\}}\right]^T = \mathbf{0} \quad (5)$$

where $[p_i^{\{\mathcal{O}\}}\ f_i^{\{\mathcal{O}\}}]^T$ $(i = 1, 2)$ is the normalized load on each beam with respect to the frame $\mathcal{O}$ attached to the center of the fixed end ($c\theta$ and $s\theta$ are short for $\cos\theta$ and $\sin\theta$, respectively). Its relationship with $[p_i\ f_i]^T$ in each beam's local frame $\mathcal{O}_i$ is ($\mathcal{O}_i$ omitted for simplicity):

$$\begin{bmatrix} p_1^{\{\mathcal{O}\}} \\ f_1^{\{\mathcal{O}\}} \end{bmatrix} = -\mathbf{R}(\frac{\pi}{2} - \beta_1)\begin{bmatrix} p_1 \\ f_1 \end{bmatrix}, \begin{bmatrix} p_2^{\{\mathcal{O}\}} \\ f_2^{\{\mathcal{O}\}} \end{bmatrix} = \mathbf{R}(\beta_2 - \frac{\pi}{2})\begin{bmatrix} p_2 \\ f_2 \end{bmatrix} \quad (6)$$

where $\mathbf{R}(\beta) = \begin{bmatrix} \mathrm{c}\beta & -\mathrm{s}\beta \\ \mathrm{s}\beta & \mathrm{c}\beta \end{bmatrix}$ is the 2D rotation matrix.

Moreover, to define the behavior of the joint, we have the geometric constraint that builds the relationship between the deflection of the two beams and the moving end:

$$\theta = \alpha_1 = \alpha_2 \quad (7)$$

$$\begin{bmatrix} w_b + w_t c\theta \\ w_b s\theta \end{bmatrix} = \mathbf{R}(\beta_2 - \frac{\pi}{2})\begin{bmatrix} x_A \\ y_A \end{bmatrix} + \mathbf{R}(\frac{\pi}{2} - \beta_1)\begin{bmatrix} x_B \\ y_B \end{bmatrix} \quad (8)$$

where $w_b = w_{1b} + w_{2b}$ and $w_t = w_{1t} + w_{2b}$ are the distances between the end of beams; $[x_A, y_A]^T$ and $[x_B, y_B]^T$ are the

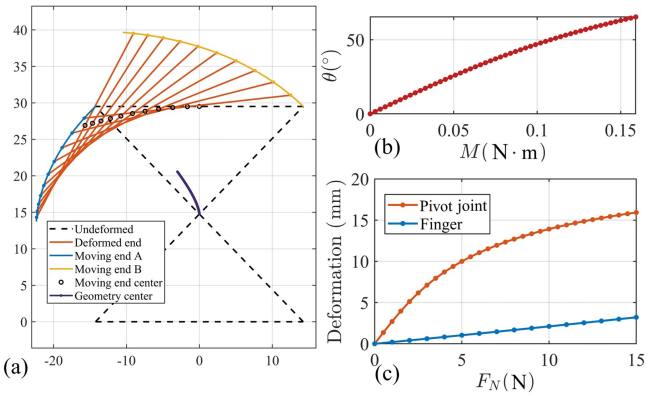

Fig. 5. Analysis of the pivot joint. (a) The deflection of the moving end in CAFP under the moment from 0 to 0.16 N·mm. (b) The relationship between the rotating and moment, indicating the stiffness. (c) Comparison of the deflection of the finger and pivot joint under the contact force.

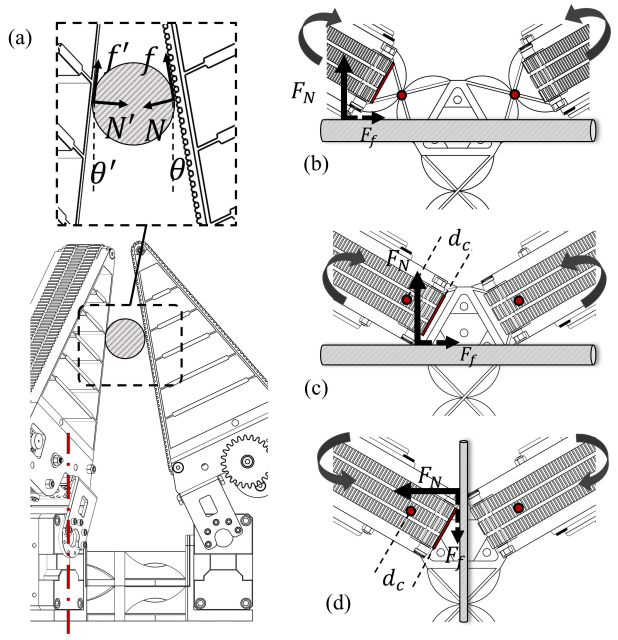

Fig. 6. Analysis of the pivot joint center. (a) Side view of three-finger grasp of an object with large a aspect ratio. (b) Successful finger pivoting during three-finger grasp. (c) Failed finger pivoting during three-finger grasp. (d) Successful finger pivoting during two-finger grasp.

end positions of each deformed beam with respect to $\mathcal{O}_2$ and $\mathcal{O}_1$ (Fig. 4(e)). So the deflection of the moving end Δx, Δy with respect to the bending angle θ is given by:

$$\begin{bmatrix}\Delta x\\ \Delta y\end{bmatrix} = -\mathbf{R}(\beta_2 - \frac{\pi}{2})\begin{bmatrix}x_A\\ y_A\end{bmatrix} + \begin{bmatrix}w_{2b}+w_{2t}c\theta\\ w_{2t}s\theta - L_2 c\beta_2\end{bmatrix} \quad (9)$$

where

$$\begin{bmatrix}x_A\\ y_A\end{bmatrix} = \begin{bmatrix}L_2\,(1+\delta x_2)\\ L_2\delta y_2\end{bmatrix}, \begin{bmatrix}x_B\\ y_B\end{bmatrix} = \begin{bmatrix}L_1\,(1+\delta x_1)\\ L_1\delta y_1\end{bmatrix} \quad (10)$$

The area moment of inertia along the beam is $I(x) = b^3 t(x)/12$ where $t(x)$ is the thickness and b is the width of the beam in the bending plane (Fig. 4(b)). The beam is designed to have a varying cross-section shape (described in (11)) to reduce the undesired twist.

$$t(x) = t_m + \left(r - \sqrt{r^2 - (L/2 - x)^2}\right), 0 \le x \le L \quad (11)$$

where $r = [(L/2)^2 + (t_b - t_m)^2]/[2\,(t_b - t_m)]$. We used the numerical average of $I(x)$ along the beam as a constant equivalent inertia I_i^{equ} to substitute for the varying I_i in the model. By solving (1)-(9), we can derive the deflection of the joint under an external load. Fig. 5(a) shows the position of the moving end under a moment exerted at its center. To reach the maximum required rotation angle for grasping, a moment of 0.139 N·m is needed (Fig. 5(b)).

2) Center of Pivot: The center of pivot (COP) is critical to the desired adaptive behavior of the pivot joint. Specifically, it is important that the location of COP allows the finger to pivot to the desired direction regardless of grasping situation.

Fig. 6(a)-(c) show common situations of three-finger grasp of an object with large a aspect ratio, where two of the fingers ideally pivot toward each other, both facing the grasped object, and the last finger stays unpivoted. Assuming the base joints of all three fingers are at the same position θ, and the pivot joints of two of the fingers have a position of $\alpha \in [30°, 90°]$. The projected angle (to the plane of the unpivoted finger) between finger and the object is given by $\theta' = \arctan(\mathrm{s}\alpha \tan\theta)$. The total normal and frictional forces of the two pivoted fingers are N' and f', respectively; and those of the unpivoted finger are N and f, where $N'(\mathrm{c}\theta' + \mu \mathrm{s}\theta') = N(\mathrm{c}\theta + \mu \mathrm{s}\theta)$, and μ is the coefficient of friction. For an object to be grasped stably within hand, we have

$$N\mathrm{s}\theta + N'\mathrm{s}\theta' \le \mu(N\mathrm{c}\theta + N'\mathrm{c}\theta') \quad (12)$$

Substituting the relationship between N and N' to the above equation gives:

$$(2\mu\,\mathrm{s}\alpha)(\tan\theta)^2 + (1-\mu^2)(1+\mathrm{s}\alpha)\tan\theta - 2\mu \le 0 \quad (13)$$

By solving (13), we can derive the value of θ that enables a stable grasp. For example, in the extreme case where $\mu = 0$, we have $\theta \le 0$. The value of θ would allow us to verify if the location of COP would allow for a desired pivot motion. As shown in Fig. 6(b), F_N applied to the finger will cause the finger to pivot in the desired direction around COP (the red dot). In general, our design allows for desired pivoting motion as long as $\theta \le 0$. The design is further verified for a similar two-finger grasping situation. As shown in Fig. 6(d), assuming F_f is negligible during pivoting, we have the following constraint of max distance that the contact point can be in front of the COP:

$$d_c \le \min\left(0.5 w_{fg} \tan(\alpha - 30°)\right) = 25.98\,\mathrm{mm} \quad (14)$$

which means the current design provides desired pivoting motions of the fingers during two-finger grasps. In the unlikely scenario where two fingers contact each other at their fingertips, as shown in Fig. 6(c), the finger will fail to pivot to the desired direction.

C. Force Limits in Grasping and Manipulation

This last subsection provides analysis results on the maximum forces of the finger and the active surfaces. Assuming an object is being grasped by all three fingers in the middle of the finger, we have $G_l = 3\mu_o \tau_{dxl}/L_c$ where G_l is the maximum weight of a grasped object, μ_o is the coefficient of friction between the belt and the object, τ_{dxl} is the maximum output torque of the motor, and L_c is the distance between the motor shaft and the contact location on the finger. An assumed $\mu_o = 0.5$ will result in $\sim$60 N of maximum weight of a grasped object. This corresponds to a $\sim$40 N normal force on the fingers, which would not cause excessive deformation of the Fin Ray mechanism based on Fig. 3(b).

To manipulate an object of maximum weight using the active surface, the torque required from the micro DC motor to actuate the belt is calculated as $\tau_{DC} = \mu_i G_l r_{pulley}/(3\mu_o \eta)$, where η is the gear ratio, μ_i is the coefficient of friction between the belt and the Fin Ray backbone, and r_{pulley} is the radius of the timing belt pulley. An assumed $\mu_i = 0.2$ will result in the required torque as $0.114\,\mathrm{N}\cdot\mathrm{m}$, which is within the permissible torque range of the motor.

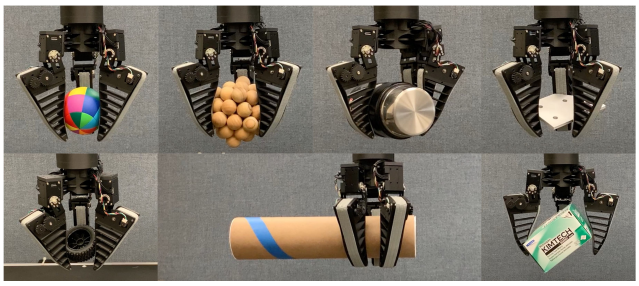

Fig. 7. Experimental objects being manipulated by BACH. (Top row left to right: a spherical puzzle, an irregularly shaped puzzle, an insulated bottle, an irregular pentagon shaped bracket; bottom row left to right: an RC car wheel, a long cylinder, a box manipulated by two fingers)

V. Experiments and Discussion

We fabricated a proof-of-concept prototype, as shown in Fig. 1, to validate the design and explore possible manipulation capabilities using various test objects (Fig. 7). The grasper was mounted on a Universal Robots UR5 robotic arm for all experiments. As described in Section III, each finger has two actuated DoFs, the base DoF and the surface DoF. The base DoF primarily provides a grasping force for the object and ensures a secure grasp; we used a position control with a current cap enforced. The surface DoF uses velocity control, and the velocity is estimated using the quadrature encoder readings filtered with a simple Kalman filter. All experiments were teleoperated.

A. Grasping

The compliant finger design and the pivotable fingers allow the hand to grasp objects of different sizes and shapes including a sphere, a long cylinder, an insulated bottle, a box, an irregular pentagon plate, an RC car wheel, and an irregularly shaped puzzle. All of these objects can be grasped with both pinch grasp and power grasp. They can also be securely grasped at different poses, which is the foundation of a stable in-hand manipulation.

The fine fingertips allow the grasper to pick up very thin objects directly from the desk with a pinch grasp. The compliant palm allows the flat finger tip to adapt to various cross-section shapes of the grasped object, without which the edges of the finger, where the friction is relatively low, will be in contact with the object and cause the object to slip. Once the fingers are aligned with the shape of the object during a pinch grasp, the active surface can draw the grasped object farther into the grasper, achieving an extremely simple transition from a pinch grasp to a more robust power grasp for additional manipulation.

B. Manipulation

Theoretically, the designed hand is able to achieve 5-DoF spatial manipulation. The only direction that it cannot achieve is rotation around vertical axes, which is a design choice as explained in Section III. In the experiment, we focused on the reorientation tasks around the horizontal axes because these tasks are difficult (or impossible in some cases) for robot arms. The detailed manipulation demonstrations are presented in the complementary video of this paper.

Because of the compliance of the pivot joints, a 3-DoF planar manipulation can be achieved using two of the grasper's three fingers. This is especially useful when the grasped object can be regarded as an extrusion of a 2D shape such as the box shown in the video. In such a situation, the two fingers will be pivoted to oppose each other, allowing for a stable manipulation.

On the other end of the spectrum, when manipulating a long object, two of the three fingers can turn towards each other, achieving a side-by-side posture and opposing the third finger placed on the other side of the object. This was demonstrated using a long cylinder and an insulated bottle.

While manipulation of objects with small aspect ratios using active surfaces have been achieved previously [4], [5], this is the first time in-hand manipulation of objects with large aspect ratios have been realized using active surfaces. Specifically, the objects are being manipulated in the directions not aligned with their extreme axes. For example, it is relatively easy to rotate a long cylinder around its longitudinal axis, but difficult around other axes. A similar argument can be applied to a thin object such as a plate or a very short cylinder.

C. Limitations

1) Object shape limitation: Because the grasping motion is achieved by the base DoF to accommodate the compliant mechanism at the palm, a power grasp cannot be achieved without relying on the palm support for objects thinner than the opening of the fingers. In such situations, however, objects can be grasped and manipulated in a pinch grasp at the cost of reduced robustness. Although it is theoretically possible to achieve a power grasp with the help of the palm surface, it is not an intended use of this hand since there is no active surface located on the palm.

2) Energy efficiency: Although the timing belt has its smooth side in contact with the Fin Ray backbone, the sliding motion between them reduces the energy efficiency of the operation. This limits the weight of the objects that can be manipulated. A heavy object will require a relatively large grasping force, resulting in a large normal force on the active surface and subsequently, a large frictional force. This would put larger stress on the micro DC motor, potentially making it more prone to failure.

VI. Conclusion and Future Work

This paper presents the design of a robot hand that allows in-hand manipulation to be achieved with power grasp through the integration of compliant mechanisms and active surfaces. This design combines the grasp stability of a compliant robot hand and dexterity from active surfaces, achieving very robust in-hand manipulation. Different aspects of the design were analyzed, and experiments with the hand were conducted using objects with various shapes and sizes for verifying the hand's grasping and manipulation capabilities. Future work includes developing various control schemes to further determine the potential of this design and exploring other design options to improve the energy efficiency.

REFERENCES

[1] I. M. Bullock and A. M. Dollar, "Classifying human manipulation behavior," in *2011 IEEE International Conference on Rehabilitation Robotics*, pp. 1–6, June 2011.

[2] A. Bhatt, A. Sieler, S. Puhlmann, and O. Brock, "Surprisingly robust in-hand manipulation: An empirical study-supplementary material," in *Robotics: Science and Systems*, 2021.

[3] O. M. Andrychowicz, B. Baker, M. Chociej, R. Józefowicz, B. McGrew, J. Pachocki, A. Petron, M. Plappert, G. Powell, A. Ray, J. Schneider, S. Sidor, J. Tobin, P. Welinder, L. Weng, and W. Zaremba, "Learning dexterous in-hand manipulation," *The International Journal of Robotics Research*, vol. 39, no. 1, pp. 3–20, 2020.

[4] S. Yuan, A. D. Epps, J. B. Nowak, and J. K. Salisbury, "Design of a roller-based dexterous hand for object grasping and within-hand manipulation," in *2020 IEEE International Conference on Robotics and Automation (ICRA)*, pp. 8870–8876, 2020.

[5] S. Yuan, L. Shao, C. L. Yako, A. Gruebele, and J. K. Salisbury, "Design and control of roller grasper v2 for in-hand manipulation," in *2020 IEEE/RSJ International Conference on Intelligent Robots and Systems (IROS)*, pp. 9151–9158, 2020.

[6] L. Birglen, T. Laliberté, and C. M. Gosselin, *Underactuated robotic hands*, vol. 40. Springer, 2007.

[7] S. Hirose and Y. Umetani, "The development of soft gripper for the versatile robot hand," *Mechanism and machine theory*, vol. 13, no. 3, pp. 351–359, 1978.

[8] R. Deimel and O. Brock, "A novel type of compliant and underactuated robotic hand for dexterous grasping," *The International Journal of Robotics Research*, vol. 35, no. 1-3, pp. 161–185, 2016.

[9] P. Datseris and W. Palm, "Principles on the development of mechanical hands which can manipulate objects by means of active control," 1985.

[10] V. Tincani, M. G. Catalano, E. Farnioli, M. Garabini, G. Grioli, G. Fantoni, and A. Bicchi, "Velvet fingers: A dexterous gripper with active surfaces," in *2012 IEEE/RSJ International Conference on Intelligent Robots and Systems*, pp. 1257–1263, IEEE, 2012.

[11] R. R. Ma and A. M. Dollar, "In-hand manipulation primitives for a minimal, underactuated gripper with active surfaces," in *International Design Engineering Technical Conferences and Computers and Information in Engineering Conference*, vol. 50152, p. V05AT07A072, American Society of Mechanical Engineers, 2016.

[12] J. M. Gómez-de Gabriel and H. A. Wurdemann, "Adaptive underactuated finger with active rolling surface," *IEEE Robotics and Automation Letters*, vol. 6, no. 4, pp. 8253–8260, 2021.

[13] S. B. Backus and A. M. Dollar, "An adaptive three-fingered prismatic gripper with passive rotational joints," *IEEE Robotics and Automation Letters*, vol. 1, no. 2, pp. 668–675, 2016.

[14] T. Laliberte, L. Birglen, and C. Gosselin, "Underactuation in robotic grasping hands," *Machine Intelligence & Robotic Control*, vol. 4, no. 3, pp. 1–11, 2002.

[15] A. M. Dollar and R. D. Howe, "The highly adaptive sdm hand: Design and performance evaluation," *The International Journal of Robotics Research*, vol. 29, no. 5, pp. 585–597, 2010.

[16] G. Palli, C. Melchiorri, G. Vassura, U. Scarcia, L. Moriello, G. Berselli, A. Cavallo, G. De Maria, C. Natale, S. Pirozzi, *et al.*, "The dexmart hand: Mechatronic design and experimental evaluation of synergy-based control for human-like grasping," *The International Journal of Robotics Research*, vol. 33, no. 5, pp. 799–824, 2014.

[17] N. T. Ulrich, "Grasping with mechanical intelligence," tech. rep., 1988.

[18] W. Crooks, G. Vukasin, M. O'Sullivan, W. Messner, and C. Rogers, "Fin ray® effect inspired soft robotic gripper: From the robosoft grand challenge toward optimization," *Frontiers in Robotics and AI*, vol. 3, p. 70, 2016.

[19] S. Abondance, C. B. Teeple, and R. J. Wood, "A dexterous soft robotic hand for delicate in-hand manipulation," *IEEE Robotics and Automation Letters*, vol. 5, no. 4, pp. 5502–5509, 2020.

[20] J.-Y. Lee, Y.-S. Seo, C. Park, J.-S. Koh, U. Kim, J. Park, H. Rodrigue, B. Kim, and S.-H. Song, "Shape-adaptive universal soft parallel gripper for delicate grasping using a stiffness-variable composite structure," *IEEE Transactions on Industrial Electronics*, vol. 68, no. 12, pp. 12441–12451, 2020.

[21] L. L. Howell, "Compliant mechanisms," in *21st century kinematics*, pp. 189–216, Springer, 2013.

[22] T. L. Thomas, V. Kalpathy Venkiteswaran, G. Ananthasuresh, and S. Misra, "Surgical applications of compliant mechanisms: a review," *Journal of mechanisms and robotics*, vol. 13, no. 2, 2021.

[23] S. Jagtap, B. Deshmukh, and S. Pardeshi, "Applications of compliant mechanism in today's world–a review," in *Journal of Physics: Conference Series*, vol. 1969, p. 012013, IOP Publishing, 2021.

[24] R. R. Ma, L. U. Odhner, and A. M. Dollar, "A modular, open-source 3d printed underactuated hand," in *2013 IEEE International Conference on Robotics and Automation*, pp. 2737–2743, IEEE, 2013.

[25] R. R. Ma and A. M. Dollar, "An underactuated hand for efficient finger-gaiting-based dexterous manipulation," in *2014 IEEE International Conference on Robotics and Biomimetics (ROBIO 2014)*, pp. 2214–2219, IEEE, 2014.

[26] L. U. Odhner, L. P. Jentoft, M. R. Claffee, N. Corson, Y. Tenzer, R. R. Ma, M. Buehler, R. Kohout, R. D. Howe, and A. M. Dollar, "A compliant, underactuated hand for robust manipulation," *The International Journal of Robotics Research*, vol. 33, no. 5, pp. 736–752, 2014.

[27] Y. Gao, X. Huang, I. S. Mann, and H.-J. Su, "A novel variable stiffness compliant robotic gripper based on layer jamming," *Journal of Mechanisms and Robotics*, vol. 12, no. 5, p. 051013, 2020.

[28] P. Bilancia, M. Baggetta, G. Berselli, L. Bruzzone, and P. Fanghella, "Design of a bio-inspired contact-aided compliant wrist," *Robotics and Computer-Integrated Manufacturing*, vol. 67, p. 102028, 2021.

[29] R. Bannasch and L. Kniese, "Manipulator tool and holding and/or expanding tool with at least one manipulator tool," Dec. 18 2012. US Patent 8,333,417.

[30] Festo, "Bionictripod with fingripper." `https://www.festo.com/rep/en_corp/assets/pdf/Tripod_en.pdf`. Accessed: 2023-02-13.

[31] X. Shan and L. Birglen, "Modeling and analysis of soft robotic fingers using the fin ray effect," *The International journal of robotics research*, vol. 39, no. 14, pp. 1686–1705, 2020.

[32] C. Armanini, I. Hussain, M. Z. Iqbal, D. Gan, D. Prattichizzo, and F. Renda, "Discrete cosserat approach for closed-chain soft robots: Application to the fin-ray finger," *IEEE Transactions on Robotics*, vol. 37, no. 6, pp. 2083–2098, 2021.

[33] S. Awtar, A. H. Slocum, and E. Sevincer, "Characteristics of beam-based flexure modules," *Journal of Mechanical Design*, vol. 129, p. 625, 2007.

[34] F. Ma and G. Chen, "Modeling large planar deflections of flexible beams in compliant mechanisms using chained beam-constraint-model," *Journal of Mechanisms and Robotics*, vol. 8, no. 2, 2016.